USCAP

ARTICLE

Check for updates

Bioglass promotes wound healing by inhibiting endothelial cell pyroptosis through regulation of the connexin 43/reactive oxygen species (ROS) signaling pathway

Kailun Zhang[1,5], Bo Chai[2,5], Hao Ji[1,5], liuqing Chen[1], Yanbing Ma[1], Lifei Zhu[2], Jingyu Xu[1], Yanqing Wu[1], Yinan Lan[3], Hao Li[4], Zhiguo Feng[2], Jian Xiao[2]✉, Hongyu Zhang[2]✉ and Ke Xu[1]✉

Bioactive glass (BG) has recently shown great promise in soft tissue repair, especially in wound healing; however, the underlying mechanism remains unclear. Pyroptosis is a novel type of programmed cell death that is involved in various traumatic injury diseases. Here, we hypothesized that BG may promote wound healing through suppression of pyroptosis. To test this scenario, we investigated the possible effect of BG on pyroptosis in wound healing both in vivo and in vitro. This study showed that BG can accelerate wound closure, granulation formation, collagen deposition, and angiogenesis. Moreover, western blot analysis and immunofluorescence staining revealed that BG inhibited the expression of pyroptosis-related proteins in vivo and in vitro. In addition, while BG regulated the expression of connexin43 (Cx43), it inhibited reactive oxygen species (ROS) production. Cx43 activation and inhibition experiments further indicate that BG inhibited pyroptosis in endothelial cells by decreasing Cx43 expression and ROS levels. Taken together, these studies suggest that BG promotes wound healing by inhibiting pyroptosis via Cx43/ROS signaling pathway.

Laboratory Investigation (2022) 102:90–101; https://doi.org/10.1038/s41374-021-00675-6

INTRODUCTION

Silicate-based bioactive glasses have an outstanding ability to bond with bones and soft tissues[1]. While Bioglass® 45S5 (BG) comprises SiO_2 45 wt%, Na_2O 24.5 wt%, CaO 24.5 wt%, and P_2O_5 6.0 wt%, it can release soluble ions such as Si, Ca, and P upon contact with wound fluid[2]. Multiple studies have shown that BG can promote wound healing;[3–5] however, the underlying mechanism remains poorly understood. It has been reported that BG could promote vascularization and accelerate wound healing[6–8]. In these cases, the studies were focused primarily on the effect of BG on the proliferation and migration of endothelial cells. It is noteworthy that during the vascularization of wound healing, endothelial cells are subject to complex wound pathological conditions including inflammation, ischemia, and hypoxia[5]. These complex pathological conditions can affect the vascularization of wound healing[9]. Interestingly, inflammation and oxidative stress could cause pyroptosis, influencing endothelial cell behavior and functionalization, and further delaying wound healing.

Pyroptosis is a type of pro-inflammatory cell death characterized by cell swelling, lysis, and release of pro-inflammatory cytokines and intracellular contents. It can be mediated by several inflammasomes, such as NLRP3[10]. The current used pyroptosis makers include caspase-1 and Gasdermin D(GSDMD)[11]. Caspase-1 can regulate the classical pyroptosis signaling pathway, and GSDMD is the effect protein of pyroptosis[12,13]. While pyroptosis is implicated in various diseases such as infectious diseases, cardiovascular diseases, traumatic brain injury (TBI), and spinal cord injury (SCI)[14], the role of pyroptosis in wound healing has yet to be determined. Lopez-Pastrana et al. have reported that inhibition of proatherogenic caspase-1 activation in endothelial cells improves angiogenesis and prognosis of ischemia[15]. Mena et al. found that the histones trigger both apoptosis and pyroptosis in endothelial colony-forming cells and inhibit their angiogenic functions[16]. Tang et al. showed that neferine inhibits LPS-ATP-induced pyroptosis in endothelial cells by blocking ROS/NLRP3/Caspase-1 signaling pathway, thereby alleviating chronic kidney disease[17]. Collectively, these observations suggest that inhibition of pyroptosis may promote wound healing, especially in the process of vascularization.

In an attempt to understand the role of pyroptosis of endothelial cells in wound healing, we investigated the effect of BG on pyroptosis signaling pathway both in vivo and in vitro. Several studies have found that the gap junction Cx43 regulates endothelial cell growth and pyroptosis. It has been reported that BG promotes wound healing by affecting Cx43-mediated endothelial cell behavior[18]. Interestingly, observational studies

[1]Institute of Life Sciences, Engineering Laboratory of Zhejiang province for pharmaceutical development of growth factors, Biomedical Collaborative Innovation Center of Wenzhou, Wenzhou University, Zhejiang, China. [2]School of Pharmaceutical Sciences, Wenzhou Wound Repair and Regeneration Key Laboratory, Cixi Biomedical Research Institute, Wenzhou Medical University, Zhejiang, China. [3]Department of Orthopedic Surgery, Lishui Central Hospital, The Fifth Affiliated Hospital of Wenzhou Medical University, Zhejiang, China. [4]Department of Orthopedics Surgery, Lishui People's Hospital, The sixth affiliated hospital of Wenzhou medical university, Lishui, Zhejiang, China. [5]These authors contributed equally: Kailun Zhang, Bo Chai, Hao Ji. ✉email: xfxj2000@126.com; st_hyz@126.com; godxu1987@163.com

Received: 30 March 2021 Revised: 22 August 2021 Accepted: 30 August 2021
Published online: 14 September 2021

identified associations between Cx43 at the wound edge and poor healing response, and local knockdown of Cx43 led to an improvement in wound closure rate and final scar appearance[19]. Cx43 plays an important role in numerous cellular processes such as growth and differentiation[20]. However, little is known about the role of Cx43 in BG-regulated pyroptosis during wound healing.

In this study, we set out to elucidate the mechanism underlying BG-stimulated wound healing. Particularly, we investigated the effects of BG ion products on wound healing rate, granulation regeneration, pyroptosis-related signaling pathways, Cx43 expression and ROS levels, while testing whether BG inhibits pyroptosis in endothelial cells via Cx43/ROS signaling. Furthermore, the present study assessed the protective effect of BG on Lipopolysaccharide-Adenosine Triphosphate (LPS-ATP) induced endothelial cell model.

MATERIALS AND METHODS

Characterization and ion release of BG

BG powder (45S5) was purchased from Ugulin (Hebei, China). The ultrastructure of BG surface was observed by scanning electron microscope (SEM) (HITACHI, Japan).

First, an appropriate amount of BG was weighed, dissolved in a simulated body fluid (SBF) (Coolaber, Beijing, USA), and mixed thoroughly for 48 h. Thereafter, the precipitate was cleaned with absolute ethanol (chromatographic grade, aladdin, China) and then freeze-dried. Finally, the surface functional groups of the samples were characterized by Fourier Transform Infrared Spectrometer (FTIR) (NICOLET, USA).

Next, 1 g BG was dissolved in 5 mL SBF. After 24 h of soaking, the supernatant was collected and passed through a 0.22 μm filter. And the BG stock solution was then diluted with serum-free endothelial cell culture medium to different titers (1/10, 1/20, 1/50, 1/100, 1/200, 1/300, and 1/500). The content of Ca, Si, and P in the BG ion extract was determined by inductively coupled plasma atomic emission spectrometry (ICPOES730, Agilent, USA).

Cell culture and treatments

Human umbilical vein endothelial cells (HUVECs) were purchased from Sciencell (California, USA). HUVECs were cultured in Endothelial Cell Medium (ECM) (Sciencell, California, USA) supplemented with 10% fetal bovine serum, 1% (v/v) penicillin/streptomycin and endothelial cell growth supplement at a constant temperature of 37 °C with 5% CO_2.

HUVECs were seeded in 96-well or 6-well plates. LPS-ATP was used to generate an in vitro injury model[17]. In the experiments, HUVECs in a serum-free medium were first treated with 1 μg/ml LPS (Beyotime, Shanghai, China) for 6 h and then stimulated with 5 mM ATP (Beyotime, Shanghai, China) for 30 min.

Cell proliferation detection

Cell proliferation was assayed by cell counting kit-8 (CCK8)[21,22]. Approximately 5000 cells were seeded per well of a 96-well plate. After incubation for 24 h, the cells were treated with the 1/200 BG for 6 h and then washed with phosphate buffered saline (PBS). Thereafter, 10 μL of CCK8 (Beyotime, Shanghai, China) solution was added to each well, and the cells were incubated for 2 h in a constant-temperature incubator at 37 °C in the dark. Next, absorbance values were measured at 450 nm with a microplate reader.

Cell death detection

Pyroptosis was evaluated by lactate dehydrogenase (LDH) release assay and propidium iodide (PI)/Hoechst staining[23]. For the LDH release assay (Mao Kang, Shanghai, China), the 96-well plate was treated with the drug for 6 h and then subjected to centrifugation at 400 *g* for 5 min. After the centrifugation, 120 μL of supernatant was removed and 60 μL of LDH detection solution was added. Thereafter, the mixture was incubated for 30 min in the dark at room temperature with gentle shaking. Finally, the absorbance values were determined at 490 nm with a microplate reader, and the LDH release was calculated by the formula: %LDH release = 100 × (Corrected reading from Test well − corrected reading from untreated well)/(Corrected maximum LDH release control − corrected reading from untreated well). In the PI/Hoechst staining (Solarbio, Beijing, China), the treated cells were collected and incubated with a staining buffer containing PI and Hoechst at 4 °C in the dark for 20–30 min. After being washed with PBS, the cells were observed and photographed with an inverted microscope.

ROS assay

The cellular ROS levels were detected by using the method of loading probes in situ[24,25]. Briefly, 10 μM of 2,7-Dichlorodi-hydrofluorescein diacetate (DCFH-DA) (Beyotime, Shanghai, China) was added to each well of a six-well plate following completion of the drug stimulation, and cells were incubated at 37 °C for 20 min. Thereafter, the cells were washed with PBS to remove unbound DCFH-DA. The six-well plates were then examined by an inverted fluorescence microscope (Leica, DM3000, Germany). Under the microscope, six fields of view were randomly selected and 300–500 cells were observed. Positive spots and non-positive spots were displayed in red and DAPI color only, respectively.

ROS levels in tissues were determined by using Dihydroethidium (DHE), one of the most commonly used superoxide anion fluorescent detection probes[6,26]. After dewaxing, rehydration, and antigen retrieval (see the immunostaining for a detailed protocol), the tissue sections were incubated with DHE dye (Beyotime, Shanghai, China) at 37 °C for 30 min, washed with PBS, and mounted with an anti-fluorescence quencher. Finally, the tissues were photographed with an upright fluorescence microscope (Zeiss, 3847010149, Germany).

Experimental animals and surgical procedures

4–6-week-old male ICR mice were provided by Wenzhou Medical University (License No. SCXK [ZJ] 2015-0009). To generate the wound model, mice were anesthetized, and the hairs on the back of the mice were shaven. Concentric fluorine rubber washers with an inner diameter of 0.8 cm, an outer diameter of 1.6 cm, and a thickness of 0.05 cm were fixed on both sides of the vertebrae of the mice by using 5-0 suture line, and then two full-layer skin wounds were made with a 6-mm round skin biopsy punch (Acuderm inc., Ft Lauderdale, FL, USA). To prevent chewing or scratching, the exposed skin was covered with a transparent dressing (3 M Health Care, Germany) and wrapped with an elastic bandage. Approximately 4 mg/cm^2 of BG powder was applied to cover the whole wound surface in the treatment group, and the negative control (NC) group only do damage treatment. The wound healing was observed on day 0, 3, 6, 9, 12, and 15 after surgery, while wound closure was measured with ImageJ. In the meantime, the same size of skin tissue was removed on the 7th day, and the number of blood vessels below the tissue was counted.

GAP134 and GAP26 have often been used respectively to activate and inhibit Cx43 gap junctions[27,28]. To investigate the effect of Cx43 on wound healing, mice were randomly divided into the four groups: normal group, NC group, GAP134 group, and GAP26 group. Both GAP134 (MCE, USA) and GAP26 (MCE, USA) were dissolved in distilled water. While GAP134 at the daily dose of 3 mg/kg was given by gavage, GAP26 was intraperitoneally injected into mice at a dose of 25 μg/kg/day[29]. As a control, distilled water was used in the other two groups.

Western blot analysis

Protein extraction from the tissue or cells was performed by using RIPA lysis solution (Beyotime, Shanghai, China) mixed with the protease inhibitor cocktail (Beyotime, Shanghai, China) and PMSF (Beyotime, Shanghai, China) at a ratio of 1:100. After centrifugation at 12,000 rpm for 15 min at 4 °C, the supernatant was collected and subjected to protein quantification. Thereafter, the proteins were separated by SDS-PAGE gel electrophoresis and then transferred to a polyvinylidene difluoride membrane (BioRad, Hercules, CA, USA). After being blocked with 5% skim milk for 2 h at room temperature, the membrane was incubated with the primary antibodies overnight at 4 °C. On the following day, the membrane was washed with TBST (Tris-buffered saline with 0.1% Tween-20) and then incubated with horseradish peroxidase-conjugated secondary antibodies (Beyotime, Shanghai, China) for 2 h at room temperature. Blots were assayed with an enhanced chemiluminescence detection kit (Bio-Rad, Hercules, CA, USA). The images were acquired with Chemi DocXRS + Imaging System (Bio-Rad), and protein bands were quantified by using the Quantity-One software.

The following primary antibodies were used in this study: NLRP3 and GSDMD (Abcam, Cambridge, UK); caspase-1, IL-18, GAPDH, β-tubulin, and Cx43 (Proteintech, Chicago, USA); and IL-1β (ABclonal, Boston, USA).

a

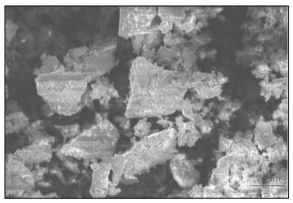

b

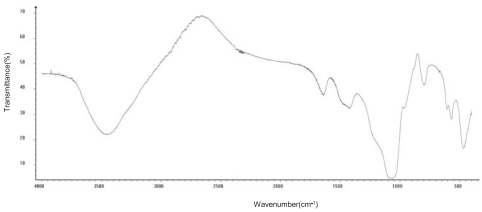

c

	Ca (mg/L)	P (mg/L)	Si (mg/L)
SBF	104.97±3.09	2.68±0.07	0.09±0.06
BG+SBF	110.43±1.21	2.71±0.06	1.22±0.03

Fig. 1 Characterization of BG. a SEM images of prepared BG particles. **b** Infrared absorption spectrum of BG immersed in SBF solution. **c** The concentration of ion in the BG extract.

Histology and immunostaining

The tissue samples were fixed in 4% paraformaldehyde for 24 h and then washed with running water for 4 h. After being dehydrated in an ethanol gradient (70, 80, 95, and 100%), the samples were finally embedded in paraffin. The wax block was cut into 5-μm sections and fixed on glass slides.

Hematoxylin and eosin (H&E) staining and Masson's trichrome staining were performed according to the instructions on the kit (Beyotime, Shanghai, China). Staining of each group was measured by the integrated optical density of stained granulation or collagen fibers per unit area using Image-J software. For the immunostaining of tissue samples, sections in the slides were dewaxed with xylene, rehydrated through an ethanol gradient, and treated using 3% H_2O_2 for 15 min. After antigen retrieval with citric acid, high temperature and high pressure, the slides were blocked with 5% BSA for 30 min at 37 °C and then incubated with the primary antibody at 4 °C overnight. On the following day, the slides were washed with TBST and subjected to an incubation with a fluorescently labeled secondary antibody at 37 °C for 2 h. Finally, the coverslips were mounted on slides with an anti-fluorescence quencher. In the immunohistochemistry staining, DAB (Beyotime, Shanghai, China) and hematoxylin (Beyotime, Shanghai, China) were used for color development and nuclear staining, respectively. The slides were mounted with a neutral gum (Beyotime, Shanghai, China).

The following antibodies and reagents were used in the tissue staining: rabbit polyclonal anti-CD31 antibodies (Abcam, Cambridge, UK), Lycopersicon Esculentum Lectin (Mao Kang, Shanghai, China), goat anti-rabbit IgG H&L (Abcam, Cambridge, UK), goat anti-mouse IgG H&L (Abcam, Cambridge, UK), and anti-fade mounting medium with DAPI (Beyotime, Shanghai, China). All images were taken with Leica microscope.

Statistical analysis

Data were shown as mean ± Standard Deviation (SD). SPSS was used for statistical analysis. While comparison between two groups was tested with Student's *t*-test method, comparisons among multiple groups were conducted by one-way analysis of variance (ANOVA). $P < 0.05$ was considered as statistically significant difference.

RESULTS

Characterization of BG

As shown on the SEM image, BG was composed of irregular particles with a particle size of 10–90 μm (Fig. 1a). Notably, the FTIR spectra of BG after immersion revealed that while the 960 cm^{-1} shoulder peak and absorption peak at 870 cm^{-1} corresponded to P–O stretching vibration and C–O bending vibration, respectively, the two strong vibration bimodal peaks at 564 and 605 cm^{-1} corresponded to P–O bending vibration peaks of the crystal phosphate basic group (Fig. 1b). The presence of these characteristic absorption peaks indicated that Hydroxy-Carbonate-Apatite (HCA) has been formed on BG surface. We next measured the concentration of ion in the BG extract. As depicted in Fig. 1c, there was little difference in the concentrations of Ca and P between SBF alone and BG-containing SBF. On the contrary, the concentration of Si detected in 1/200 BG was much higher than that in SBF, while little Si was present in SBF. These data demonstrated that the concentration of Si was in the range of 1.19–1.25 mg/L.

BG accelerates wound closure and promotes neovascularization in mice

In order to determine the effect of BG on skin wound healing, we comparatively assessed the wound conditions at various time points between the NC group and BG group. As shown in Fig. 2a, b, starting from the 3rd day, the BG group displayed a significantly smaller size of wound than the NC group. Moreover, the daily wound closure rate in BG group was markedly higher than that in NC group, while BG group exhibited the best closing effect on the 15th day of the wound. In the meantime, we performed tissue section staining on the 15th day. As depicted in Fig. 2c–e, while the BG group had a shorter wound length, the granulation tissue formation and collagen deposition were approximately twice as much as the NC group, which were reminiscent of those processes in normal tissue. Conversely, we observed sparser granulation tissue formation and collagen deposition in NC group compared with BG group. Collectively, these results indicated that BG can accelerate wound closure probably through promoting the regeneration and deposition of granulation and collagen.

We further investigated the effect of BG on blood vessel formation as well as the underlying mechanism. As shown in Fig. 2f, g, the BG group had higher blood vessel density and aggregation degree at the edge of the wound than NC group. The immunostaining assay revealed that while the BG group had abundant blood vessels, it developed mature ring blood vessels as indicated by the circularity structure composed of CD31 positive spots. All these findings demonstrated that BG can not only accelerate granulation formation and collagen deposition, but also promote angiogenesis and development toward normal tissues.

BG suppresses pyroptosis in vivo

It has been shown that pyroptosis plays an important negative regulatory role in angiogenesis[15]. A number of factors including NLRP3, activated caspase-1, GSDMD, cleaved IL-1β, and cleaved IL-18 can be markedly upregulated in pyroptosis[23]. To determine whether pyroptosis inhibition is involved in accelerated wound healing mediated by BG, western blot analysis was conducted to examine the expression levels of pyroptosis-related proteins. As

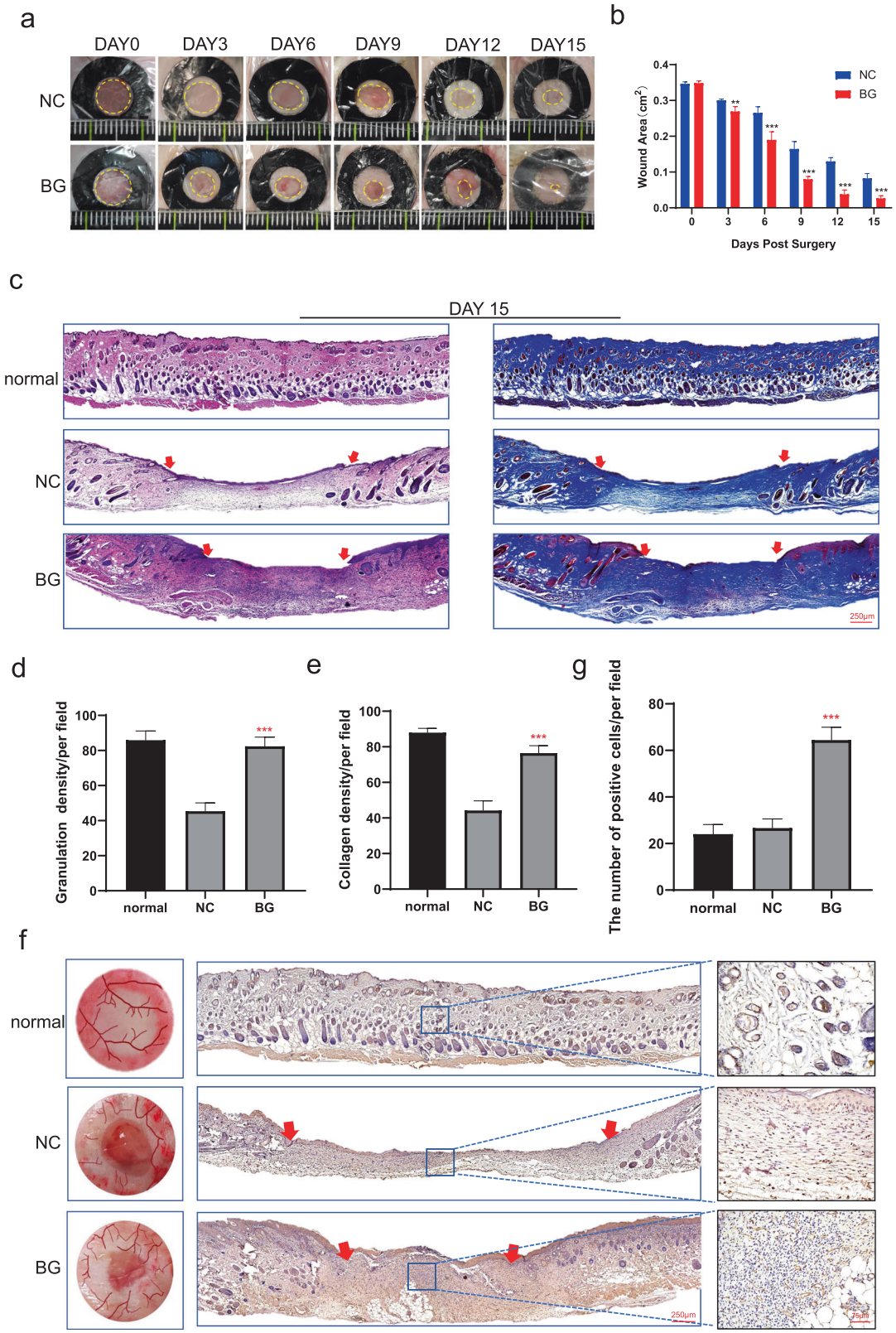

Fig. 2 BG accelerates wound closure and promotes neovascularization in mice. a Representative images of wounds in the NC and BG groups at various time points after surgery (day 0, 3, 6, 9, 12, and 15). **b** Statistical analysis of wound areas in the two groups at different time points. $^{**}P < 0.01$ and $^{***}P < 0.001$ vs. NC group, $n = 5$. **c**–**e** Hematoxylin and Eosin (H&E) staining and Masson staining were conducted at day 15 after surgery to examine granulation formation and collagen deposition. Scale bar = 250 μm, $n = 3$. $^{***}P < 0.001$ vs. NC group. **f**, **g** Assessment of vascularization of skin wounds and representative images of CD31 immunostaining of the wound tissue on the 7th day after surgery. Scale bar = 250, 75 μm, $n = 5$. $^{***}P < 0.001$ vs. NC group.

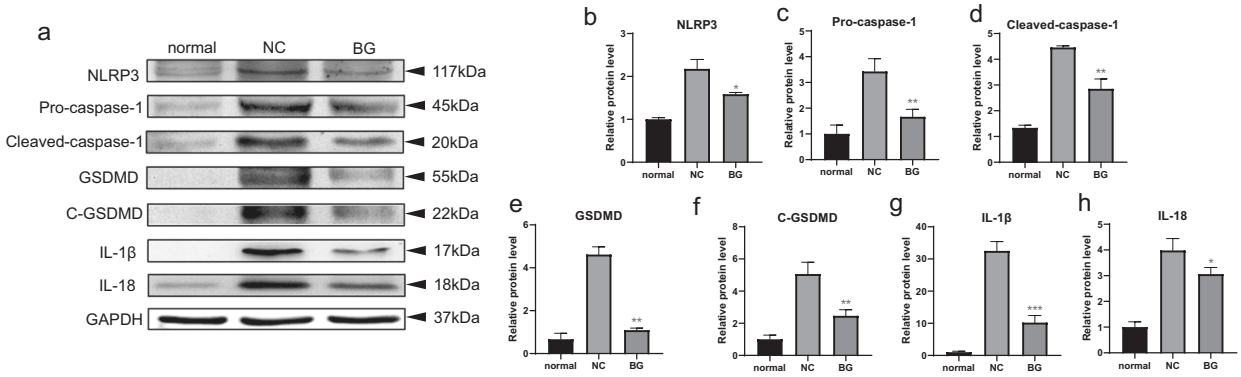

Fig. 3 BG suppresses pyroptosis in vivo. a Western blotting was performed to analyze the expression of pyroptosis-related proteins in the normal group, NC group and BG group on day 7 after surgery. **b**–**h** Quantitative analysis of pyroptosis-related proteins expression levels in each group compared with normal group. $^{*}P < 0.05$, $^{**}P < 0.01$, and $^{***}P < 0.001$ vs. NC group, $n = 3$.

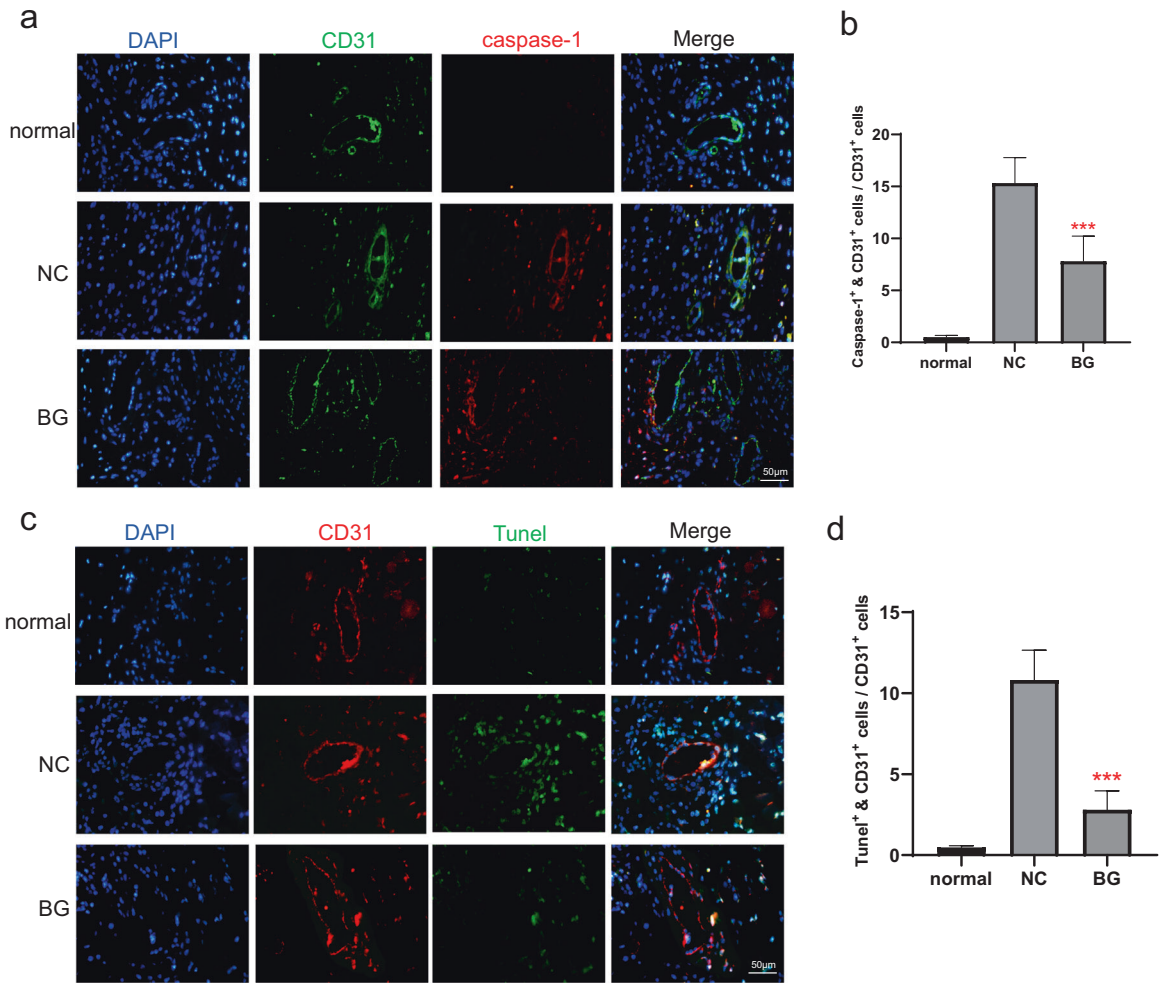

Fig. 4 BG suppresses pyroptosis in endothelial cells. a, **b** Double-immunofluorescence staining was performed to assay the expression and distribution of caspase-1 and CD31 in skin tissues from the wound edge in mice on the 7th day after surgery. Six fields of view were randomly selected for each sample, and ~200–300 cells were observed. Scale bar = 50 μm. $^{***}P < 0.001$ vs. NC group, $n = 6$. **c**, **d** TUNEL/CD31 double staining was conducted to quantitatively analyze DNA fragmentation in skin tissues from the wound edge on the 7th day after surgery. Six fields of view were randomly selected for each sample, and ~200–300 cells were observed. Scale bar = 50 μm. $^{***}P < 0.001$ vs. NC group, $n = 6$.

shown in Fig. 3a–h, compared with the normal group, the expression levels of pyroptosis-related proteins were apparently increased in the NC group. Strikingly, treatment with BG for 7 days led to a remarkable decrease in the protein expression levels. Thus, we performed caspase-1/CD31 and TUNEL/CD31 double staining to further analyze pyroptosis in vascular endothelial cells. The immunostaining revealed more caspase-1-positive endothelial cells the NC group as compared to the BG group (Fig. 4a, b). Moreover, the BG group displayed a significantly lower percentage of TUNEL-positive cells than the NC group (Fig. 4c, d). Together,

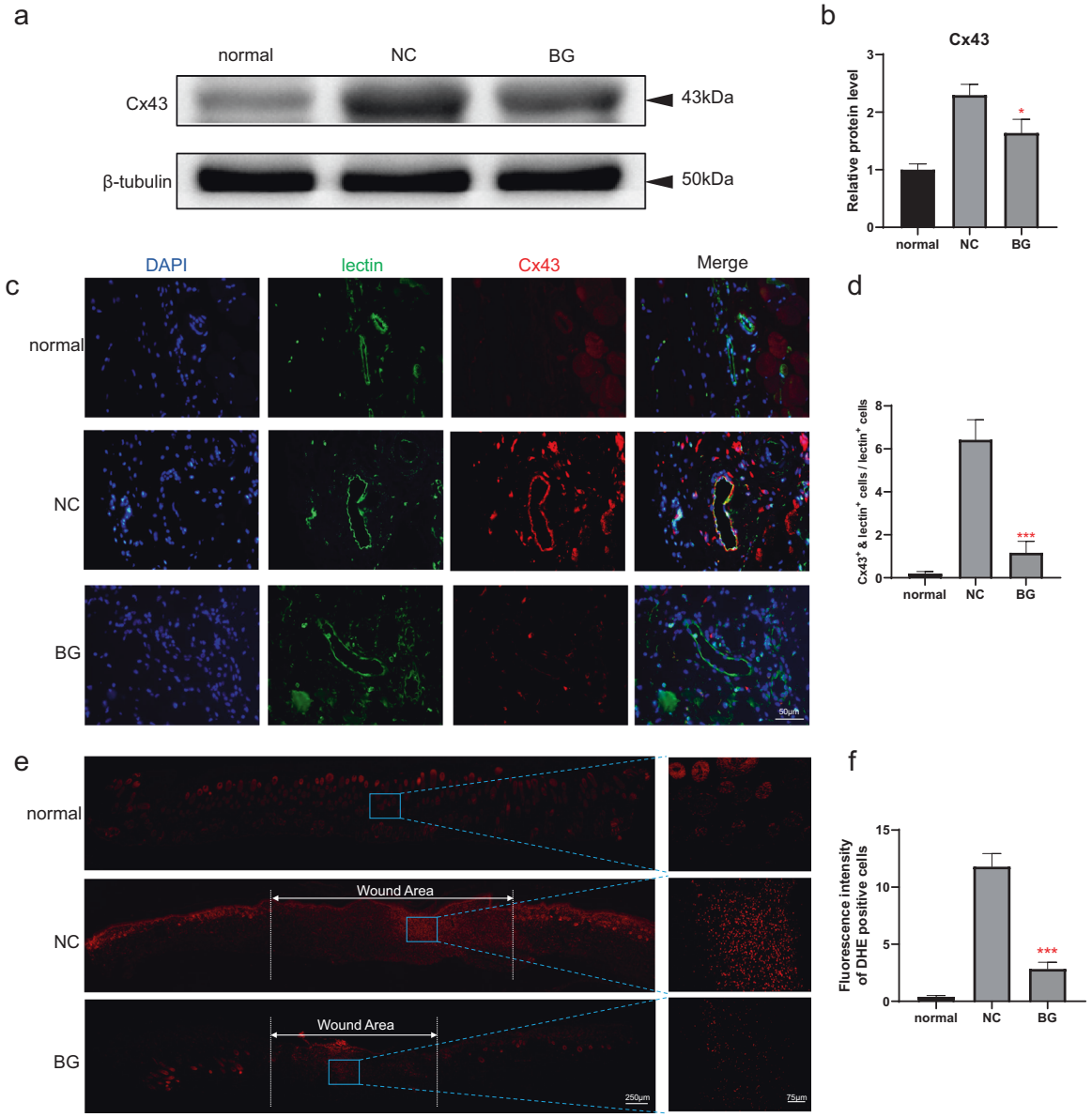

Fig. 5 BG affects Cx43 expression and ROS levels. a Western blotting was conducted to detect the expression of Cx43 in different groups at day 7 after surgery. Six fields of view were randomly selected for each sample, and ~200–300 cells were observed. **b** Quantitative analysis of the protein expression of Cx43 compared with the normal group. *$P < 0.05$ vs. NC group, $n = 3$. **c**, **d** Cx43/CD31 double staining was performed to assay Cx43 expression in endothelial cells from the wound edge on the 7th day after surgery. Scale bar = 50 μm. ***$P < 0.001$ vs. NC group, $n = 6$. **e**, **f** ROS levels in the wound area were measured by using a ROS probe (dihydroethidium, DHE) with different treatments. Scale bar = 250, 75 μm. ***$P < 0.001$ vs. NC group, $n = 3$.

these results suggested that BG is capable of suppressing pyroptosis in endothelial cells.

BG affects Cx43 expression and ROS levels

Previous studies have shown that ROS can induce pyroptosis[17], while Cx43, the main connexin of vascular gap junction communication, regulates ROS levels[30], and BG affects the expression of Cx43[18]. Based on these observations, we speculated that Cx43 and ROS might be involved in BG-mediated wound healing. To verify this assumption, we first analyzed the levels of Cx43 and ROS in tissue. As shown in Fig. 5a, b, while normal skin tissues had low expression of Cx43, Cx43 expression was increased in the NC group. Notably, BG treatment decreased the expression of Cx43 to almost the same level as that in the normal group. Meanwhile, co-staining of Cx43 and CD31 showed that compared with the NC group, Cx43-positive spots accumulated on the endothelial cells were significantly decreased in tissue (Fig. 5c, d). We next performed DHE staining to measure ROS levels in skin tissues. The staining revealed that under the condition of removing the background color interference (normal group), the red fluorescence at the wound was markedly reduced in BG group compared with the NC group, indicating that BG was able to scavenge ROS (Fig. 5e, f). Taken together, these data demonstrated that BG can downregulate Cx43 expression as well as ROS levels.

Effects of GAP134 and GAP26 on wound healing in mice

To further investigate whether BG accelerates wound healing through inhibiting pyroptosis in endothelial cells via Cx43/ROS signaling, we examined the wound and downstream signaling pathways in mice administered with Cx43 activator (GAP134) or Cx43 inhibitor (GAP26). The analysis showed that compared with

the NC group, GAP134 group displayed less granulation formation and sporadic cell distribution below the wound, while GAP26 group had more complete wound healing and formed a dense granulation layer by a large number of cells and capillaries (Fig. 6a). As depicted in Fig. 6b–e, we further observed that GAP134 treatment led to an increase in the expression levels of Cx43, whereas GAP26 downregulated Cx43 expression. Moreover, GAP26 could inhibit pyroptosis-related proteins more effectively than GAP134. In addition, the DHE staining revealed that GAP134 increased ROS levels while GAP26 did not (Fig. 6f, g). Collectively, these observations suggest that BG promoted the wound healing may be related to the Cx43/ROS-mediated endothelial cell pyroptosis pathway.

BG rescues LPS-ATP-induced pyroptosis in HUVECs

To detect the toxicity of BG, the BG extract was serially diluted with serum-free endothelial cell culture medium to different titers (1/10, 1/20, 1/50, 1/100, 1/200, 1/300, and 1/500), and the effect of different concentrations of BG extract on HUVECs was examined. Clearly, SBF alone had no effect on proliferation of HUVECs, excluding the interference of different concentrations of SBF in the assays (Fig. S1a). As depicted in Fig. 7a, compared with the control group, the high concentrations of BG extract (1/10, 1/20, and 1/50) displayed an inhibitory effect on proliferation of HUVECs, while the low concentrations of BG extract (1/100, 1/200, 1/300, and 1/500) barely had effect on HUVECs.

Next, we performed in vitro experiments to investigate the effect of BG on pyroptosis in HUVECs. In the experiments, LPS-ATP was used to induce pyroptosis in the cells as described previously[17]. HUVECs were treated with various concentrations of BG to determine the suitable therapeutic concentration. As shown in Fig. 7b, treatment with BG at a dilution of 1/100 or 1/200 led to a favorable cell survival and effectively decreased LPS-ATP-induced cell damage. This observation was consistent with data on LDH release (Fig. 7c). Thus, these findings identified 1/100 and 1/200 BG as the suitable concentrations for rescuing LPS-ATP-induced damage in HUVECs. Data showed that different concentrations of SBF had no therapeutic effect on endothelial cell pyroptosis induced by LPS-ATP (Fig. S1b), Thus, the results could not be explained by an effect of SBF. We further assessed pyroptosis by using PI/Hoechst staining. The staining showed a marked reduction in the number and intensity of red fluorescence in the BG group as compared to LPS-ATP group, indicating that the BG group had much less cell death caused by cell rupture (Fig. 7d, e). To better understand pyroptosis in HUVECs, western blot analysis was carried out. As shown in Fig. 7f–m, while the expression levels of NLRP3, cleaved-caspase-1, C-GSDMD, IL-1β, and IL-18 were significantly increased in LPS-ATP-treated HUVECs, further incubation of the HUVECs with 1/200 BG resulted in reduction in the levels of those pyroptosis-related proteins. This study, therefore, provided more evidence that BG can rescue pyroptosis in endothelial cells.

BG inhibits pyroptosis in HUVECs by downregulating Cx43 and ROS levels

To prove that BG suppressed pyroptosis in endothelial cells via Cx43/ROS, we comparatively analyzed the expression levels of Cx43 in different groups. As shown in Fig. 8a, b, the expression level of Cx43 in the LPS-ATP group was remarkedly higher than that in the BG group, indicating a role of BG in reducing Cx43 expression in HUVECs. Moreover, the ROS staining identified fewer red positive spots in the BG group, showing that BG can effectively alleviate the oxidative stress of HUVECs induced by LPS-ATP (Fig. 8c, d). Combined with the in vivo results, the in vitro assays support the notion that BG alleviates pyroptosis in endothelial cells by decreasing Cx43 expression and ROS levels.

DISCUSSION

It has been reported that BG can enhance granulation regeneration, inhibit inflammation, and promote cell migration and proliferation in wound healing, accelerating wound healing[4,5,31]. While BG has triggered much interest in its applications for wound healing, the mechanism underlying the role of BG in the process remains unclear. Formation of a functional blood vessel network via angiogenesis is an essential step of wound healing. Angiogenic cytokines, cell types, and the extracellular matrix (ECM) have been identified as crucial factors in blood vessel formation. Given that inhibition of pyroptosis caused further vascularization in many animal models, it can be reasoned that BG may enhance vascularization through inhibiting pyroptosis. Although studies on gap junctions have been conducted to understand BG-mediated stimulatory effects on vascularization, effects of BG on gap junction and pyroptosis in endothelial cells have yet to be determined. As Cx43 affects pyroptosis in different cell types in response to various stimuli, it remains to be resolved whether BG inhibits downstream signaling pathway of pyroptosis via Cx43 in wound healing. In this study, we have demonstrated that the BGs affect Cx43 expression and ROS production, thereby inhibiting the downstream signaling pathway of pyroptosis both in vivo and in vitro (Fig. 9).

Topological structure of biomaterials is important in affecting cell behaviors[32]. In the present study, we showed that biologically active BG causes sequential physical and chemical effects upon contact with the skin and soft tissue wounds, forming a hydroxyapatite layer with a porous network structure, which has physical adsorption capacity[33–35]. Moreover, we observed that BG has certain biological induction properties. In this case, it can absorb and recruit a large number of tissue regeneration related proteins as well as various healing-promoting factors, accelerating wound healing through promoting granulation tissue formation and collagen deposition (Fig. 2). In addition, BG can form an alkaline microenvironment on the wound surface due to ion dissolution, which prevents some pathogenic bacteria from surviving on the surface in the early stage of wound healing, plays antibacterial and anti-inflammatory effects, and contributes to wound healing[1,36–38]. While this layer of HCA structure has been shown to play a key role in cell behavior, the underlying mechanism remains unclear.

As channels for nutrient and energy transport, blood vessels play a vital role in the process of wound repair. After a few days of proliferation and migration of vascular endothelial cells, the entire granulation tissue is filled with microvascular networks that effectively promote the healing of skin wounds[8,39]. Furthermore, multiple studies have shown that BG-mediated angiogenesis is indispensable for promoting wound healing[18,37]. Wu et al. found that BG can generate a gentle and cell-friendly microenvironment for mesenchymal stem cells and their ionic products, which promotes endothelial cell vascularization and facilitates intradermal angiogenesis[40]. Gendy et al. reported that BG can induce the differentiation of dental pulp stromal cells into endothelial cells[41]. Moreover, two separate studies demonstrated that 45S5 ion products can promote macrophage phenotype conversion (M1 to M2) by slowing down the inflammatory response of the wound, while repairing intercellular paracrine effects. As a result, 45S5 ion products not only activate more anti-inflammatory factors and angiogenic growth factors, but also boost the migration of endothelial cells and fibroblasts, and increase the formation of capillary-like network of endothelial cells as well as the deposition of ECM proteins of fibroblasts[6,42]. Consistent with the above observations, the present study found that BG continuously stimulates the formation of granulation tissue for providing vascular endothelial cells with a suitable growth environment, triggering a large number of blood vessels to extend near the wound for the nutrient supply of the surrounding cells and tissues. These observations were consistent with the results in Fig. 2.

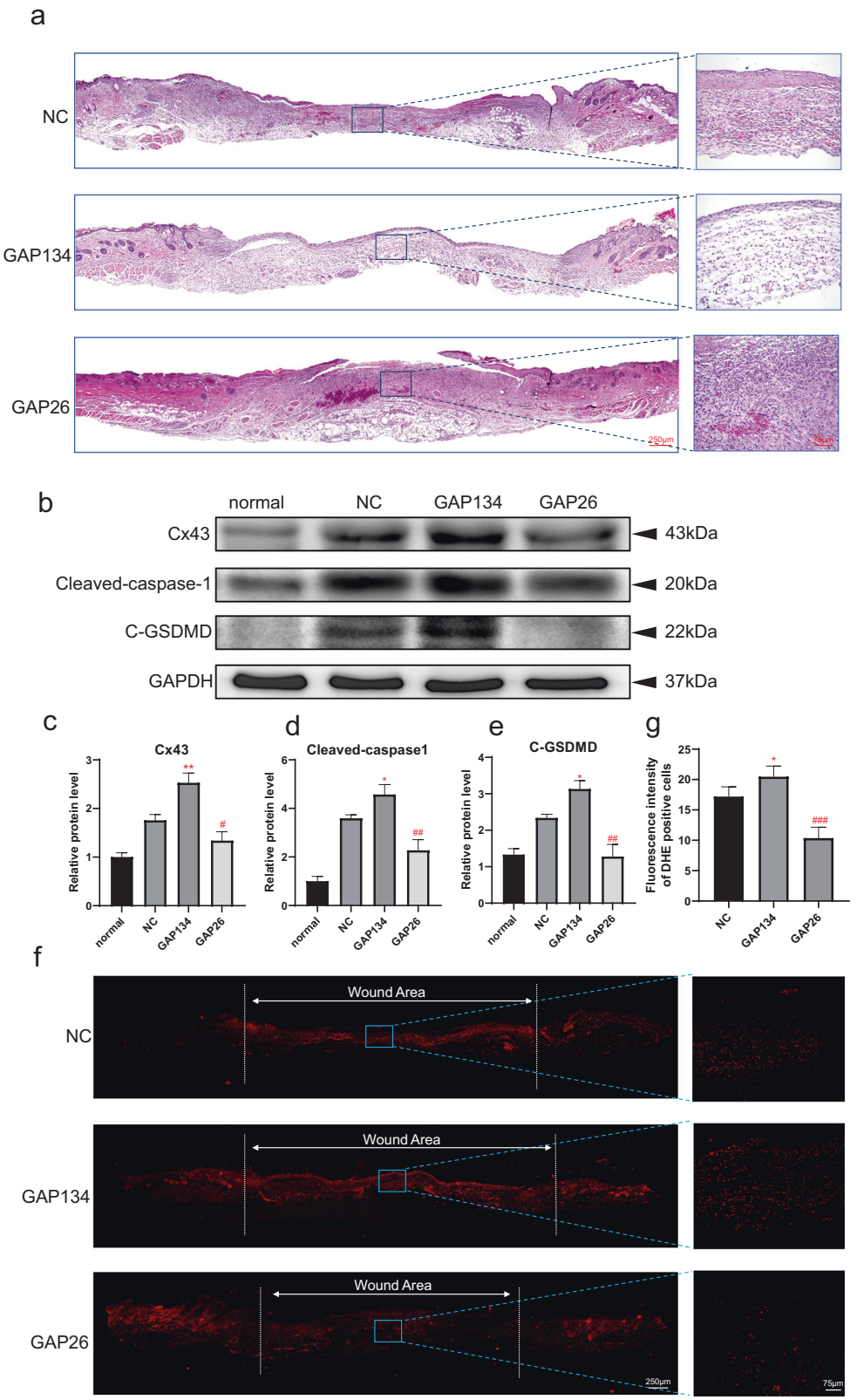

Fig. 6 Effects of GAP134 and GAP26 on wound healing in mice. a HE staining was performed to evaluate the extent of granulation formation in the NC group, GAP134 group, and GAP26 group on the 7th day after surgery. Scale bar = 250, 75 μm, $n = 3$. **b** Western blotting was conducted to detect the expression of Cx43 and pyroptosis-related proteins in different groups at day 7 after surgery. **c**–**e** Quantitative analysis of Cx43 and pyroptosis-related proteins expression levels in each group compared with normal group. $^{*}P < 0.05$, $^{**}P < 0.01$, $^{\#}P < 0.05$, and $^{\#\#}P < 0.01$ vs. NC group, $n = 3$. **f**, **g** ROS levels in different tissues were assayed by using DHE staining. Scale bar = 250, 75 μm. $^{*}P < 0.05$ and $^{\#\#\#}P < 0.001$ vs. NC group, $n = 3$.

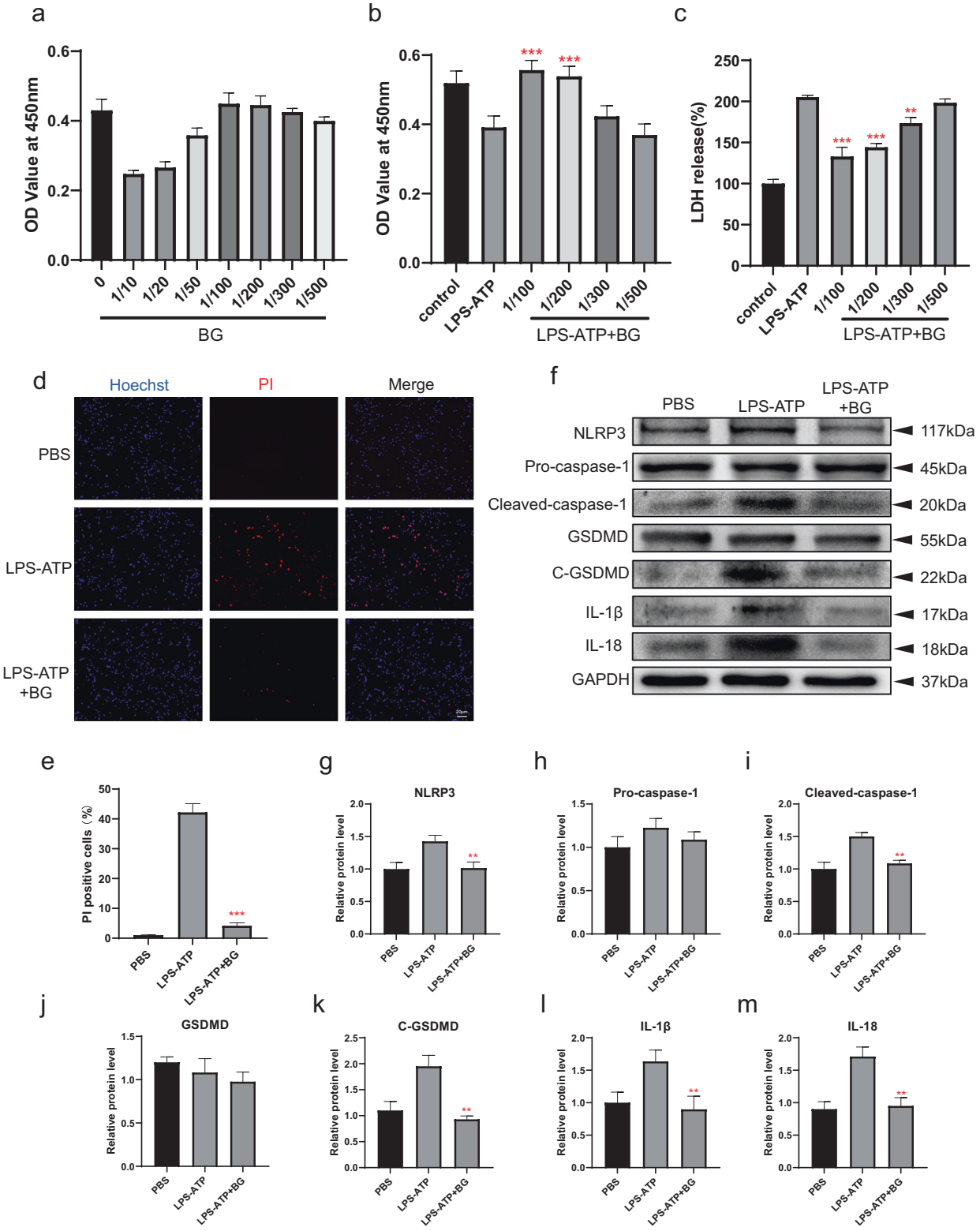

Fig. 7 BG rescues LPS-ATP-induced pyroptosis in HUVECs. a The effect of BG ion extract diluted with serum-free ECM in different ratios from 1/10 to 1/500 on cell proliferation, $n = 6$. **b** Effects of various concentrations of BG on proliferation of HUVECs treated with LPS-ATP. ***$P <$ 0.001 vs. LPS-ATP group, $n = 6$. **c** LDH release in HUVECs treated with LPS-ATP plus different concentrations of BG was assayed. **$P < 0.01$ and ***$P < 0.001$ vs. LPS-ATP group, $n = 3$. **d**, **e** Hoechst/PI staining was performed to detect the percentage of PI-positive cells in HUVECs. Scale bar = 20 μm. ***$P < 0.001$ vs. LPS-ATP group, $n = 6$. **f** Western blotting was conducted to analyze the expression of pyroptosis-related proteins in LPS-ATP-stimulated HUVECs treated with 1/200 of BG. **g**–**m** Quantitative analysis of the expression of pyroptosis-related proteins in each group compared with control. **$P < 0.01$ vs. LPS-ATP group, $n = 3$.

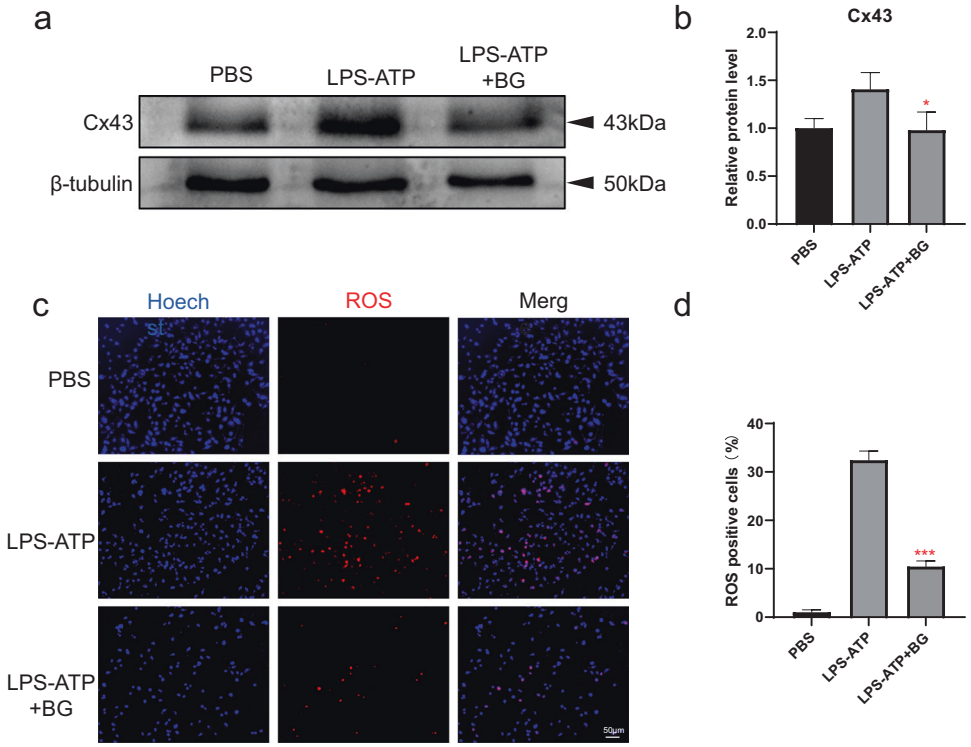

Fig. 8 BG inhibits pyroptosis in HUVECs by downregulating Cx43 expression and ROS levels. a Western blotting was performed to detect the expression of Cx43 in different groups. **b** Quantitative analysis of the protein expression of Cx43 compared with the control. *$P < 0.05$ vs. LPS-ATP group, $n = 3$. **c**, **d** Hoechst/ROS staining was conducted to detect the percentage of ROS-positive cells in HUVECs. Scale bar = 50 μm. ***$P < 0.001$ vs. LPS-ATP group, $n = 6$.

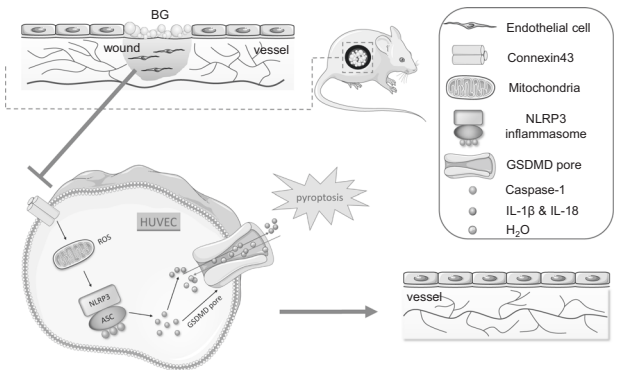

Fig. 9 Schematic diagram showing that BG promotes wound healing by inhibiting endothelial cell pyroptosis through regulating Cx43/ROS signaling pathway. Upon contact of BG with wound body fluid, HCA structure is formed on the surface through ion exchange. Downregulating the Cx43 protein on endothelial cells could reduce the level of ROS activity, thereby inhibit the activation of caspase-1 by NLRP3 inflammasome, weaken the punching activity of GSDMD, and finally suppress endothelial cell pyroptosis. Subsequently, promoted formation of blood vessels leads to acceleration of wound healing.

Wound healing does not occur properly in harsh environments such as ischemia and hypoxia; however, the underlying mechanism remains elusive.

There are several types of cell–cell junctions with a unique function found in epithelia, including tight junctions, adhesive junctions, gap junctions, and desmosomes[43,44]. Intercellular interactions mediated by gap junctions are involved in the regulation of endothelial cell function during vascular inflammation. Among them, the gap junction Cx43 has been showed to play a key role in the communication between endothelial cells. Cx43 allows electrical synchronization and small molecule exchange between the adjacent cells, reduces the permeability of cell monolayers, affects blood vessel function, and hinders wound healing[45–47]. Thuringer et al. reported that functional gap junctions composed of Cx43 enable the formation of cancer cells and human microvascular endothelial cells, while upregulation of Cx43 expression could inhibit its ability in promoting angiogenesis[48]. Cx43 has been shown to exert a regulatory effect on endothelial cells. Strikingly, we and others demonstrated that BG can affect the expression of Cx43 in endothelial cells[6]. However, these studies were very superficial and did not thoroughly explore the function of gap junction protein and how it affected wound healing. Zou et al. found that inhibiting Cx43 can suppress ROS transfer and inactivate JNK1/Sirt1/FoxO3a signaling pathway, thereby preventing intestinal damage caused by sepsis[30]. Ding et al. observed that Cx43 can mediate ROS transfer between adjacent vascular endothelial cells[49]. Gao et al. concluded that ROS activates oxidation-sensitive kinase p38 prior to the onset of cell damage and causes the switch of Cx43 from non-phosphorylated form to highly phosphorylated form[50]. Similarly, Ma et al. found that Cx43 overexpression increases ROS levels and promotes apoptosis in the LPS model in which endothelial cells are stimulated[51] . Obviously, ROS is a key factor in wound microenvironment. Inhibition of ROS production is conducive to cell growth, and there is a very close relationship between connexin 43 and ROS. In the present study, we showed that BG inhibits the expression of Cx43, downregulating downstream ROS, promoting the formation of new blood vessels, and accelerating the healing of wounds (Figs. 2 and 5). In the meantime, in vitro experiments in the study provided evidence that BG extract downregulates the expression of Cx43 in endothelial cells in the injured environment, while reducing function of ROS in wound healing (Fig. 8).

Pyroptosis is a pro-inflammatory type of programmed cell death with characteristics of both apoptosis and necrosis. Caspase-1 is activated during pyroptosis by inflammasomes (NACHT, LRR, PYD). Subsequently, the punching activity is produced, which leads to the change of osmotic pressure, and induces the synthesis and release of various inflammatory factors and adhesion factors. Finally local amplification makes the systemic inflammatory response[52]. Previous studies have identified an essential role of pyroptosis in trauma repair. TBI is similar to wound injury in terms of pathophysiological mechanisms. It has been reported that while pyroptosis inhibits brain repair through NLRP3 and caspase-1 mediated cellular inflammation, the mechanisms also involve neuroinflammation and neuronal damage following TBI[53–55]. Dai et al. suggested an involvement of pyroptosis in inflammation of the spinal cord after SCI, which may be related to inhibition of microglia activation and pyroptosis pathway[56]. While biomaterials with anti-inflammatory effects like BG could probably inhibit pyrostosis and apoptosis through certain signaling pathways (Figs. 3, 4, and 7), studies on pyrostosis in wound repair are still lacking. Most of the cells in the wound fail to grow normally due to various pressures and injuries. As one of the links, ROS has been showed to be closely related to pyrostosis. A large number of literatures reported that ROS is the upstream signal molecule of pyrostosis, which was verified by ROS scavenger experiments. Even cell experiments also confirmed that oxidative stress of endothelial cells could regulate pyrostosis effectively[17,57–59]. Given an established relationship between Cx43, ROS and pyrostosis[60], we further investigated how they are functionally involved in BG-accelerated wound healing.

In this study, we used Cx43 activators and inhibitors to determine how Cx43 is involved in inhibition of pyroptosis linked to BG-promoted wound healing. It has been demonstrated that GAP134 and GAP26 act as the activator and inhibitor of gap junctions Cx43, respectively[27–29,61–63]. Here, we found that GAP26 facilitates granulation formation and accelerates wound healing by reducing ROS levels as well as pyroptosis, while GAP134 does not (Fig. 6). To verify the effects of Cx43 on wound healing identified by using Cx43 activators and inhibitors, further studies on transgenic mice are needed.

CONCLUSION

This study showed that BG application in the wound led to an enhancement of granulation tissue formation, collagen deposition and angiogenesis, accelerating development toward normal skin. Moreover, we observed that BG can inhibit pyroptosis, while downregulating Cx43 and ROS signaling pathways to promote skin healing. Besides, in vitro experiments revealed that while BG supernatant had no effect on proliferation of HUVECs, 1/200 of BG extract in the LPS-ATP injury model can significantly downregulate Cx43 expression and ROS levels in HUVECs and inhibit pyroptosis. All these results indicate that BG inhibits pyroptosis by regulating Cx43/ROS signaling pathway, promotes the formation of new blood vessels, and accelerates wound healing.

DATA AVAILABILITY

The data used to support the findings of this study are available from the corresponding author upon request.

REFERENCES

1. Rizwan, M., Hamdi, M. & Basirun, W. J. Bioglass® 45S5-based composites for bone tissue engineering and functional applications. *J. Biomed. Mater. Res. A.* **105**, 3197–3223 (2017).
2. Kumar, A., Murugavel, S., Aditya, A. & Boccaccini, A. R. Mesoporous 45S5 bioactive glass: synthesis, in vitro dissolution and biomineralization behavior. *J. Mater. Chem. B.* **5**, 8786–8798 (2017).
3. Wu, C. et al. Preparation and characterization of borosilicate-bioglass-incorporated sodium alginate composite wound dressing for accelerated full-thickness skin wound healing. *Biomed. Mater.* **15**, 055009 (2020).
4. Yu, H., Peng, J., Xu, Y., Chang, J. & Li, H. Bioglass activated skin tissue engineering constructs for wound healing. *ACS Appl. Mater. Interfaces.* **8**, 703–715 (2016).
5. Kong, L. et al. Bioactive injectable hydrogels containing desferrioxamine and bioglass for diabetic wound healing. *ACS Appl. Mater. Interfaces.* **10**, 30103–30114 (2018).
6. Dong, X., Chang, J. & Li, H. Bioglass promotes wound healing through modulating the paracrine effects between macrophages and repairing cells. *J. Mater. Chem. B.* **5**, 5240–5250 (2017).
7. Zhou, Y. et al. Bioglass Activated Albumin Hydrogels for Wound Healing. *Adv. Healthc Mater.* **7**, e1800144 (2018).
8. Tonnesen, M. G., Feng, X. & Clark, R. A. Angiogenesis in wound healing. *J. Investig. Dermatol. Symp. Proc.* **5**, 40–46 (2000).
9. Opneja, A., Kapoor, S. & Stavrou, E. X. Contribution of platelets, the coagulation and fibrinolytic systems to cutaneous wound healing. *Thromb. Res.* **179**, 56–63 (2019).
10. Xue, Y., Enosi Tuipulotu, D., Tan, W. H., Kay, C. & Man, S. M. Emerging Activators and Regulators of Inflammasomes and Pyroptosis. *Trends Immunol* .**40**, 1035–1052 (2019).
11. Frank, D. & Vince, J. E. Pyroptosis versus necroptosis: similarities, differences, and crosstalk. *Cell Death Differ.* **26**, 99–114 (2019).
12. Man, S. M., Karki, R. & Kanneganti, T. D. Molecular mechanisms and functions of pyroptosis, inflammatory caspases and inflammasomes in infectious diseases. *Immunol. Rev.* **277**, 61–75 (2017).
13. Lu, F. et al. Emerging insights into molecular mechanisms underlying pyroptosis and functions of inflammasomes in diseases. *J. Cell Physiol.* **235**, 3207–3221 (2020).
14. Hu, X. et al. Role of Pyroptosis in Traumatic Brain and Spinal Cord Injuries. *Int. J. Biol Sci.* **16**, 2042–2050 (2020).
15. Lopez-Pastrana, J. et al. Inhibition of Caspase-1 Activation in Endothelial Cells Improves Angiogenesis: A NOVEL THERAPEUTIC POTENTIAL FOR ISCHEMIA. *J. Biol. Chem.* **290**, 17485–17494 (2015).
16. Mena, H. A. et al. Extracellular histones reduce survival and angiogenic responses of late outgrowth progenitor and mature endothelial cells. *J. Thromb. Haemost.* **14**, 397–410 (2016).
17. Tang, Y. S. et al. Neferine inhibits LPS-ATP-induced endothelial cell pyroptosis via regulation of ROS/NLRP3/Caspase-1 signaling pathway. *Inflamm Res.* **68**, 727–738 (2019).
18. Li, H., He, J., Yu, H., Green, C. R. & Chang, J. Bioglass promotes wound healing by affecting gap junction connexin 43 mediated endothelial cell behavior. *Biomaterials.* **84**, 64–75 (2016).
19. Montgomery J., Ghatnekar G. S., Grek C. L., Moyer K. E., Gourdie R. G. Connexin 43-Based Therapeutics for Dermal Wound Healing. *Int. J. Mol. Sci.* **19**, 1778 (2018).
20. Shi, Q. et al. Connexin Controls Cell-Cycle Exit and Cell Differentiation by Directly Promoting Cytosolic Localization and Degradation of E3 Ligase Skp2. *Dev. Cell.* **35**, 483–496 (2015).
21. Hou, G. et al. An activated mTOR/p70S6K signaling pathway in esophageal squamous cell carcinoma cell lines and inhibition of the pathway by rapamycin and siRNA against mTOR. *Cancer Lett.* **253**, 236–248 (2007).
22. Cheng, S. T., Chen, Z. F. & Chen, G. Q. The expression of cross-linked elastin by rabbit blood vessel smooth muscle cells cultured in polyhydroxyalkanoate scaffolds. *Biomaterials.* **29**, 4187–4194 (2008).
23. Jia, C. et al. Endothelial cell pyroptosis plays an important role in Kawasaki disease via HMGB1/RAGE/cathespin B signaling pathway and NLRP3 inflammasome activation. *Cell Death Dis.* **10**, 778 (2019).
24. Zou, J. et al. Deoxyelephantopin induces reactive oxygen species-mediated apoptosis and autophagy in human osteosarcoma cells. *Cell Physiol. Biochem.* **42**, 1812–1821 (2017).
25. Jia, S. J. et al. Lysophosphatidylcholine-induced elevation of asymmetric dimethylarginine level by the NADPH oxidase pathway in endothelial cells. *Vascul. Pharmacol.* **44**, 143–148 (2006).
26. Wang, S. et al. Nanoenzyme-reinforced injectable hydrogel for healing diabetic wounds infected with multidrug resistant bacteria. *Nano Lett.* **20**, 5149–5158 (2020).
27. Patin, J. et al. Gap-134, a Connexin43 activator, prevents age-related development of ventricular fibrosis in Scn5a(+/)(-) mice. *Pharmacol. Res.* **159**, 104922 (2020).
28. Desplantez, T., Verma, V., Leybaert, L., Evans, W. H. & Weingart, R. Gap26, a connexin mimetic peptide, inhibits currents carried by connexin43 hemichannels and gap junction channels. *Pharmacol. Res.* **65**, 546–552 (2012).
29. Yang, K. et al. Synaptic plasticity after focal cerebral ischemia was attenuated by Gap26 but enhanced by GAP-134. *Front. Neurol.* **11**, 888 (2020).

30. Zou, Z. et al. Cx43 inhibition attenuates sepsis-induced intestinal injury via downregulating ROS transfer and the activation of the JNK1/Sirt1/FoxO3a signaling pathway. *Mediators Inflamm.* **2019**, 7854389 (2019).
31. Naseri, S., Lepry, W. C. & Nazhat, S. N. Bioactive glasses in wound healing: hope or hype? *J. Mater. Chem. B* **5**, 6167–6174 (2017).
32. Lyu, Z. et al. Maintaining the pluripotency of mouse embryonic stem cells on gold nanoparticle layers with nanoscale but not microscale surface roughness. *Nanoscale* **6**, 6959–6969 (2014).
33. Hench, L. L. & Jones, J. R. Bioactive glasses: frontiers and challenges. *Front. Bioeng. Biotechnol* **3**, 194 (2015).
34. Hench, L. L. The story of Bioglass. *J. Mater. Sci. Mater Med.* **17**, 967–978 (2006).
35. Verrier, S., Blaker, J. J., Maquet, V., Hench, L. L. & Boccaccini, A. R. PDLLA/Bioglass composites for soft-tissue and hard-tissue engineering: an in vitro cell biology assessment. *Biomaterials* **25**, 3013–3021 (2004).
36. Rodrigues, C. et al. Bioglass 45S5: Structural characterization of short range order and analysis of biocompatibility with adipose-derived mesenchymal stromal cells in vitro and in vivo. *Mater. Sci. Eng. C Mater. Biol. Appl* **103**, 109781 (2019).
37. Handel, M., Hammer, T. R., Nooeaid, P., Boccaccini, A. R. & Hoefer, D. 45S5-Bioglass (®)-based 3D-scaffolds seeded with human adipose tissue-derived stem cells induce in vivo vascularization in the CAM angiogenesis assay. *Tissue Eng. Part A* **19**, 2703–2712 (2013).
38. Hu, S., Chang, J., Liu, M. & Ning, C. Study on antibacterial effect of 45S5 Bioglass. *J. Mater. Sci. Mater. Med.* **20**, 281–286 (2009).
39. Xu, K. et al. Topical application of fibroblast growth factor 10-PLGA microsphere accelerates wound healing via inhibition of ER stress. *Oxid. Med. Cell Longev.* **2020**, 8586314 (2020).
40. Wu, Z., He, D. & Li, H. Bioglass enhances the production of exosomes and improves their capability of promoting vascularization. *Bioact. Mater.* **6**, 823–835 (2021).
41. El-Gendy, R. et al. Investigating the vascularization of tissue-engineered bone constructs using dental pulp cells and 45S5 bioglass(R) scaffolds. *Tissue Eng. Part A* **21**, 2034–2043 (2015).
42. Ma, Z., Song, W., He, Y. & Li, H. Multilayer injectable hydrogel system sequentially delivers bioactive substances for each wound healing stage. *ACS Appl. Mater. Interfaces* **12**, 29787–29806 (2020).
43. Bazzoni, G. & Dejana, E. Endothelial cell-to-cell junctions: molecular organization and role in vascular homeostasis. *Physiol. Rev.* **84**, 869–901 (2004).
44. Garcia M. A., Nelson W. J., Chavez N. Cell-cell junctions organize structural and signaling networks. *Cold Spring Harb Perspect Biol* **10**, a029181 (2018).
45. Zou, X. R., Tao, J. & Wang, Y. K. [Gap junction and diabetic foot]. *Zhejiang Da Xue Xue Bao Yi Xue Ban* **44**, 684–688 (2015).
46. Okamoto, T. et al. Gap junction-mediated regulation of endothelial cellular stiffness. *Sci. Rep.* **7**, 6134 (2017).
47. Kim, D., Mouritzen, U., Larsen, B. D. & Roy, S. Inhibition of Cx43 gap junction uncoupling prevents high glucose-induced apoptosis and reduces excess cell monolayer permeability in retinal vascular endothelial cells. *Exp. Eye Res.* **173**, 85–90 (2018).
48. Thuringer, D. et al. Gap junction-mediated transfer of miR-145-5p from microvascular endothelial cells to colon cancer cells inhibits angiogenesis. *Oncotarget* **7**, 28160–28168 (2016).
49. Ding, H., Jiang, Y., Jiang, Y., Yuan, D. & Xiao, L. Ulinastatin attenuates monocyte-endothelial adhesion via inhibiting ROS transfer between the neighboring vascular endothelial cells mediated by Cx43. *Am. J. Transl. Res.* **12**, 4326–4336 (2020).
50. Gao, K. et al. A novel TXNIP-based mechanism for Cx43-mediated regulation of oxidative drug injury. *J. Cell Mol. Med.* **19**, 2469–2480 (2015).
51. Ma, J. W., Ji, D. D., Li, Q. Q., Zhang, T. & Luo, L. Inhibition of connexin 43 attenuates oxidative stress and apoptosis in human umbilical vein endothelial cells. *BMC Pulm. Med.* **20**, 19 (2020).
52. LaRock, C. N. & Cookson, B. T. Burning down the house: cellular actions during pyroptosis. *PLoS Pathog.* **9**, e1003793 (2013).
53. Liu, W. et al. Ablation of caspase-1 protects against TBI-induced pyroptosis in vitro and in vivo. *J. Neuroinflammation* **15**, 48 (2018).
54. Sun, Z. et al. VX765 Attenuates Pyroptosis and HMGB1/TLR4/NF-κB Pathways to Improve Functional Outcomes in TBI Mice. *Oxid. Med. Cell Longev.* **2020**, 7879629 (2020).
55. Kuwar, R. et al. A novel small molecular NLRP3 inflammasome inhibitor alleviates neuroinflammatory response following traumatic brain injury. *J. Neuroinflammation* **16**, 81 (2019).
56. Dai, W. et al. Celastrol inhibits microglial pyroptosis and attenuates inflammatory reaction in acute spinal cord injury rats. *Int. Immunopharmacol.* **66**, 215–223 (2019).
57. Abais, J. M., Xia, M., Zhang, Y., Boini, K. M. & Li, P. L. Redox regulation of NLRP3 inflammasomes: ROS as trigger or effector? *Antioxid. Redox. Signal* **22**, 1111–1129 (2015).
58. Wu, X. et al. Nicotine promotes atherosclerosis via ROS-NLRP3-mediated endothelial cell pyroptosis. *Cell Death Dis.* **9**, 171 (2018).
59. Zhou, B. et al. Tom20 senses iron-activated ROS signaling to promote melanoma cell pyroptosis. *Cell Res.* **28**, 1171–1185 (2018).
60. Huang, Y. et al. Connexin43 Contributes to Inflammasome Activation and Lipopolysaccharide-Initiated Acute Renal Injury via Modulation of Intracellular Oxidative Status. *Antioxid. Redox. Signal* **31**, 1194–1212 (2019).
61. Li, X. et al. Inhibition of connexin43 improves functional recovery after ischemic brain injury in neonatal rats. *Glia* **63**, 1553–1567 (2015).
62. Butera, J. A. et al. Discovery of (2S,4R)-1-(2-aminoacetyl)-4-benzamidopyrrolidine-2-carboxylic acid hydrochloride (GAP-134)13, an orally active small molecule gap-junction modifier for the treatment of atrial fibrillation. *J. Med. Chem.* **52**, 908–911 (2009).
63. Hawat, G., Benderdour, M., Rousseau, G. & Baroudi, G. Connexin 43 mimetic peptide Gap26 confers protection to intact heart against myocardial ischemia injury. *Pflugers Arch.* **460**, 583–592 (2010).

AUTHOR CONTRIBUTIONS

K.X., K.Z., H.J. and H.Z. were involved in the design and execution of experiments, data analysis, and manuscript writing. B.C., L.C., Y.M., L.Z., J.X., Y.L., Y.W., J.X., H.L. and Z.F. were all involved in the execution of experiments and data analysis. All authors provided the final approval of the version to be submitted.

FUNDING

This study was jointly supported by the National Natural Science Foundation of China (81802251, 81772450, and 81801233), Zhejiang Provincial Natural Science Foundation of China (LQ18H150003, LQ18H090011, LY19H150001 LY17H090014, and LWY20H310001), Zhejiang Provincial Medical and Health Science and Technology Fund (2018KY186), and Wenzhou science and technology innovation project (ZY2020023 and ZY2020026).

COMPETING INTERESTS

The authors declare no competing interests.

ETHICS STATEMENT

The animal study was reviewed and approved by the animal welfare and usage management regulations of the Wenzhou Medical University [License No. SCXK [ZJ] 2015-0009].

ADDITIONAL INFORMATION

Supplementary information The online version contains supplementary material available at https://doi.org/10.1038/s41374-021-00675-6.

Correspondence and requests for materials should be addressed to Jian Xiao, Hongyu Zhang or Ke Xu.